



Heterometallic Mg–Ba Hydride Clusters in Hydrogenation Catalysis

Michael Wiesinger,^[a] Christian Knüpfer,^[a] Holger Elsen,^[a] Jonathan Mai,^[a] Jens Langer,^[a] and Sjoerd Harder^{*[a]}

Reaction of a $\text{MgN}''_2/\text{BaN}''_2$ mixture ($\text{N}'' = \text{N}(\text{SiMe}_3)_2$) with PhSiH_3 gave three unique heterometallic Mg/Ba hydride clusters: $\text{Mg}_5\text{Ba}_4\text{H}_{11}\text{N}''_7 \cdot (\text{benzene})_2$ (1), $\text{Mg}_4\text{Ba}_7\text{H}_{13}\text{N}''_9 \cdot (\text{toluene})_2$ (2) and $\text{Mg}_7\text{Ba}_{12}\text{H}_{26}\text{N}''_{12}$ (3). Product formation is controlled by the Mg/Ba ratio and temperature. Crystal structures are described. While 3 is fully insoluble, clusters 1 and 2 retain their structures in aromatic solvents. DFT calculations and AIM analyses indicate highly ionic bonding with Mg–H and Ba–H bond paths. Also

unusual $\text{H}^- \cdots \text{H}^-$ bond paths are observed. Catalytic hydrogenation with MgN''_2 , BaN''_2 and the mixture $\text{MgN}''_2/\text{BaN}''_2$ has been studied. Whereas MgN''_2 is only active in imine hydrogenation, alkene and alkyne hydrogenation needs the presence of Ba. The catalytic activity of the $\text{MgN}''_2/\text{BaN}''_2$ mixture lies in general between that of its individual components and strong cooperative effects are not evident.

Introduction

Since the isolation of the first defined Ca hydride complex,^[1] the focus in alkaline earth (Ae) metal hydride chemistry has been on the isolation of defined, metal pure complexes. At present, molecular Ae metal hydride complexes throughout group 2 are known.^[2–5] Going down the group, increasing dynamics and ligand exchange reactions make it more challenging to isolate stable Ae metal hydride complexes. After a report on the first Mg hydride complex,^[6] various Mg hydride complexes have been fully characterized.^[4] While there are also ample examples for Ca hydride complexes,^[5] well-defined heavier Sr^[7–13] and Ba^[7,14,15] hydride complexes are few and remain a curiosity.

The fascination for Ae metal hydride complexes stems from their very high reactivity and versatility in synthesis of a large range of complexes.^[16] They are also regarded intermediates in hydrogenation catalysis, a field that underwent rapid growth and development.^[16–27] Their applications also include hydrogenation of challenging arenes,^[26,28] Hydrogen-Isotope-Exchange,^[29] C–F bond activation,^[30–32] ethylene polymerization,^[11] and controlled reactions with olefins to isolate first examples of Ca alkyls and a Sr ethyl complex.^[11,33] However, looking back at the beginnings of Ae hydride

chemistry, the research field was pioneered by a heterobimetallic system. Mulvey's heterobimetallic $[\text{M}_2\text{Mg}_2\text{H}_2(\text{N}''\text{Pr}_2)_4 \cdot (\text{toluene})_2]$ clusters ($\text{M} = \text{Na}, \text{K}$) are described as inverse crown ethers forming a ring of metals that encapsulate hydride anions (Scheme 1, A).^[34,35] Alternatively they may be seen as two magnesiate anions, $(i\text{Pr}_2\text{N})_2\text{MgH}^-$, that are bridged by two M^+ alkali metal cations. Heterobimetallic magnesium hydride systems were further explored by Hill and co-workers, who identified the bisamide stabilized structures of $\text{K}_2\text{Mg}_2\text{H}_2\text{N}''_4$ and $\text{Na}_6\text{Mg}_6\text{H}_{10}\text{N}''_8$ ($\text{N}'' = \text{N}(\text{SiMe}_3)_2$, Scheme 1, B–C).^[36] These were obtained by simple reaction of MN'' ($\text{M} = \text{Na}, \text{K}$), $\text{Mg}(n\text{Bu})_2$, and HN'' in toluene and subsequent treatment with PhSiH_3 . Most recently, Mulvey and co-workers reported crystal structures of $\text{M}_2\text{Mg}_2\text{H}_2\text{N}''_4 \cdot (\text{benzene})_x$ ($\text{M} = \text{Na}, x = 0$; $\text{M} = \text{K}, \text{Rb}, x = 2$) (Scheme 1, B and D).^[37] These heterometallic complexes have been evaluated for catalytic activity in alkene transfer hydrogenation of olefins, a methodology recently introduced by our group.^[23]

The vast majority of heterometallic s-block metal complexes are mixtures of alkali metals with either group 1, group 2, Zn or p-block metals.^[38–41] There is also a fast growing trend to disclose structures and reactivities of heterometallic s/d-block combinations.^[42–51] With focus on main group chemistry, however, the blend of two group 2 metals seems to be largely unstudied. There is a rare example for Mg/Ca hydride complex (Figure 1, E) which was isolated from a mixture of $[(\text{D}^{\text{IPP}}\text{BDI})\text{Mg}^+]$ $[\text{Al}\{\text{OC}(\text{CF}_3)_3\}_4^-]$ and $[(\text{D}^{\text{IPP}}\text{BDI})\text{CaH}]_2$.^[52] The workup is tedious, involving mechanical separation of single crystals, and the compound was poorly defined in solution. Its contamination with a by-product limited analytical investigations and reactivity studies.

Most recently, Okuda and co-workers presented a mixed Ca/Sr hydride complex (Figure 1, F).^[13] The complex appears to be the first fully characterized example of a two alkaline earth metal hydride blend that has been thoroughly studied.

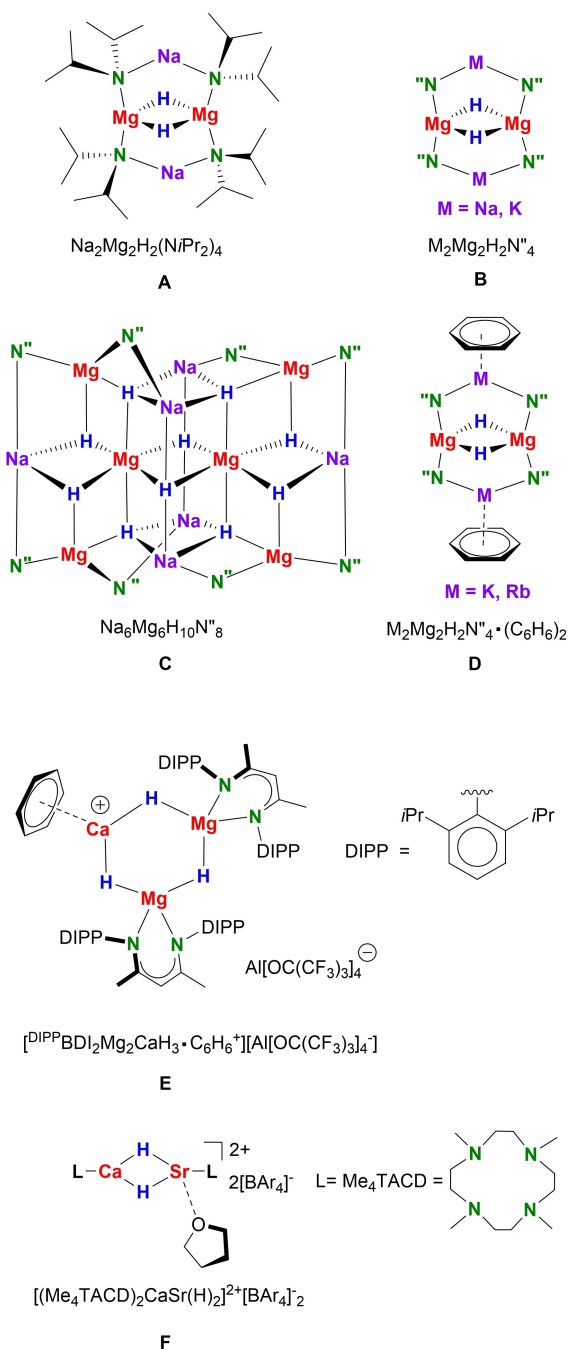
We recently demonstrated that stabilization of well-defined Ae metal hydrides not necessarily needs large bulky ligands. In

[a] M. Wiesinger, C. Knüpfer, Dr. H. Elsen, J. Mai, Dr. J. Langer, Prof. S. Harder
Inorganic and Organometallic Chemistry
Universität Erlangen-Nürnberg
Egerlandstraße 1
91058, Erlangen (Germany)
E-mail: sjoerd.harder@fau.de
Homepage: <https://www.harder-research.com>

Supporting information for this article is available on the WWW under <https://doi.org/10.1002/cctc.202101071>

This publication is part of a joint Special Collection with EurJIC on "Main Group Catalysis". Please check the ChemCatChem homepage for more articles in the collection.

© 2021 The Authors. ChemCatChem published by Wiley-VCH GmbH. This is an open access article under the terms of the Creative Commons Attribution License, which permits use, distribution and reproduction in any medium, provided the original work is properly cited.



Scheme 1. Heterometallic hydride complexes (A–F).

combination with multidentate amine ligands, the much smaller $(\text{Me}_3\text{Si})_2\text{N}$ anion, abbreviated in here as N'' , was able to stabilize a variety of Ca and Sr hydride complexes, also in solution.^[12] For Ba we could even abstain from stabilizing multidentate ligands. The heptamer (HBaN''_7) crystallized in a reasonable yield of 51% and is stable in aromatic solvents.^[15] Herein we extend this self-assembly concept to heterobimetallic Ae metal hydrides. We focused hereby on Mg^{2+} , a hard Lewis acid, and Ba^{2+} , a soft metal cation. The rationale behind this choice is that the hard-soft combination may be advantageous

in hydrogenation catalysis, with the softer metal binding the substrate and the harder metal delivering the hydride. Similar observations have been made for Li/Al hydride catalysts.^[53–55] We herein present synthesis and structures of well-defined Mg/Ba hydride clusters, which could be seen as potential intermediates during hydrogenation catalysis, and explore the effect of Mg/Ba metal-mixing in hydrogenation catalysis.

Results and discussion

Syntheses

Monitoring the reaction of MgN''_2 and BaN''_2 in an approximately 1/1 ratio with PhSiH_3 (20 °C, C_6D_6) by ^1H NMR spectroscopy showed immediate conversion of the N'' anions to $\text{PhSiH}_2\text{N}''$. During the reaction some precipitate was formed but this redissolved within minutes upon stirring. Concentrating the solution led to colorless crystals which were identified as $\text{Mg}_5\text{Ba}_4\text{H}_{11}\text{N}''_7 \cdot (\text{benzene})_2$ (**1**, yield: 46%); Scheme 2.

The ^1H NMR spectrum of a similar reaction of $\text{MgN}''_2/\text{BaN}''_2$ in a 1/2 ratio with PhSiH_3 (20 °C, C_6D_6) showed apart from cluster **1** a second species. Removal of **1** by extensive washing with pentane and subsequent crystallization from benzene afforded colorless crystals which were identified as $\text{Mg}_4\text{Ba}_7\text{H}_{13}\text{N}''_9 \cdot (\text{benzene})_2$ (**2**, 34% yield). The crystal quality of this product is poor and high quality crystals were obtained by recrystallization from toluene to give $\text{Mg}_4\text{Ba}_7\text{H}_{13}\text{N}''_9 \cdot (\text{toluene})_2$ (**2**). Although the metal/hydride ratio in both clusters **1** and **2** is more or less similar (**1**: Ae/H = 0.82, **2**: Ae/H = 0.85), the second cluster is clearly richer in Ba (**1**: Mg/Ba = 1.25, **2**: Mg/Ba = 0.57).

In an attempt to optimize reaction conditions in favor for the larger cluster, the reaction was performed at higher temperatures. Reaction of $\text{MgN}''_2/\text{BaN}''_2$ in a circa 1/2 ratio with PhSiH_3 (C_6D_6) at room temperature showed ^1H NMR signals for **1** and **2**. Prolonged heating did not affect the cluster **1**, which seems thermally quite stable, but led to gradual disappearance of **2**. Some formation of BaN''_2 seems to occur along with the appearance of trace compounds (see ESI, Figure S15–S16). However, after 12 hours of heating, crystals of a highly insoluble product could be isolated from the hot reaction mixture. This product was identified as $\text{Mg}_7\text{Ba}_{12}\text{H}_{26}\text{N}''_{12}$ (**3**), a cluster which like **2** is rich in Ba (Mg/Ba = 0.58) but clearly less rich in hydrides (Ae/H = 0.73). Total crystalline yield could be increased when hexane was used as solvent (70 °C, 12 h). However, elemental analysis was found not fully consistent with calculated values of **3**. Multiple assessments of single crystals obtained from the reaction mixture using X-ray diffraction each confirmed the identity of **3**, but with bulk purity in question, we refrain from giving a numerical yield.

Crystal structures

Complex $\text{Mg}_5\text{Ba}_4\text{H}_{11}\text{N}''_7 \cdot (\text{benzene})_2$ (**1**) crystallizes as a cluster (Figure 1a) in which the Mg_5Ba_2 -core could be best described as a pentagonal bipyramid with five equatorial Mg centers, each

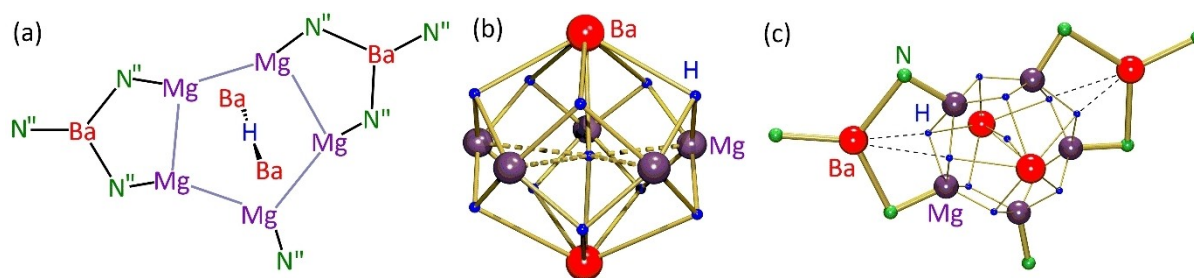
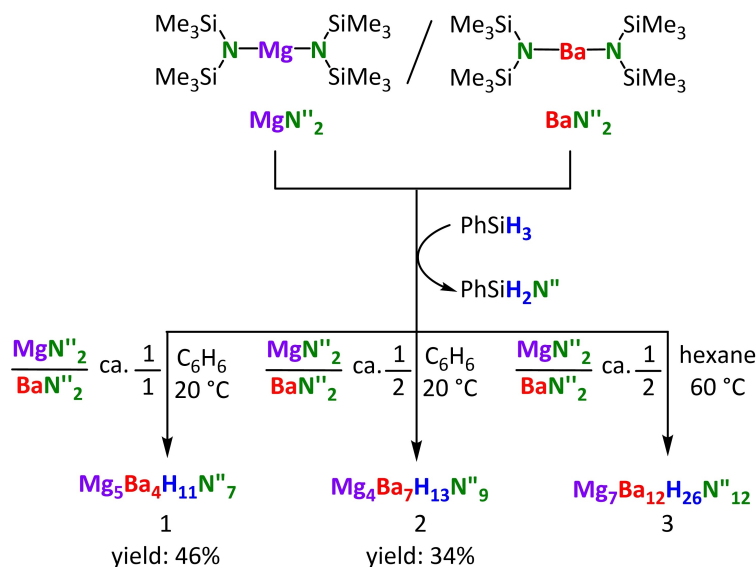


Figure 1. Crystal structure of $\text{Mg}_5\text{Ba}_4\text{H}_{11}\text{N}_7$ (1). (a) Schematic representation. (b) The $[(\text{MgH}_2)_5(\text{Ba}_2\text{H})]^{3+}$ core of 1. (c) Structure of 1 with non-hydride H atoms and Me_3Si groups omitted for clarity.



Scheme 2. Syntheses of heterometallic Mg/Ba hydride clusters (1–3).

bound to a N'' ligand, and two axial Ba centers which are both capped by benzene (Figure 1b). The ten triangular Mg_2Ba -faces each contain a μ_3 -bridging hydride and the remaining hydride is located in the center of the pyramid and is best described as an interstitial hydride.^[56,57] The two remaining $\text{N}''\text{Ba}^+$ cations bridge between two $\text{N}''\text{Mg}$ units, breaking the five-fold symmetry of the cluster. Alternatively, the complex could be thought build up from a central $(\text{C}_6\text{H}_6)\text{Ba}-\text{H}-\text{Ba}(\text{C}_6\text{H}_6)^{3+}$ spindle

surrounded by a neutral $(\text{MgH}_2)_5$ -belt in which each Mg^{2+} cation carries a N'' ligand from which two out of five are bridged by $\text{N}''\text{Ba}^+$ (Figure 1c). Although the complex does not have crystallographic symmetry, it is approximately mirror symmetric (C_s). All hydride ligands were localized and freely refined.

The Ba–H bond distances to the ten outer H^- ligands are in the range of 2.43(6)–2.86(5) Å. Those to the interstitial H^- ligand range from 2.49(6) to 2.60(6) Å; Table 1. This compares well with

Table 1. Selected bond lengths (Å) in complexes 1–3. Bold values are average values.					
$\text{Mg}_5\text{Ba}_4\text{H}_{11}\text{N}_7 \cdot (\text{benzene})_2$ (1)		$\text{Mg}_4\text{Ba}_7\text{H}_{13}\text{N}_9 \cdot (\text{toluene})_2$ (2)		$\text{Mg}_7\text{Ba}_{12}\text{H}_{26}\text{N}_{12}$ (3)	
Mg–H _{outer}	1.84(4)–2.09(7)	Mg–H _{outer}	1.88(5)–2.09(6)	Mg–H	1.87(3)–2.07(4)
	1.96		1.97		1.97
Mg–H _{center}	2.25(6)–2.87(6)	Mg–H _{center}	2.95(6)–3.21(5)		
	2.51		3.07		
Ba–H _{outer}	2.43(6)–2.86(5)	Ba–H _{outer}	2.43(6)–2.74(6)	Ba–H	2.51(2)–2.83(3)
	2.60		2.60		2.66
Ba–H _{center}	2.49(6)–2.60(6)	Ba–H _{center}	2.75(6)–2.88(6)		
	2.55		2.82		
H _{outer} ⋯H _{outer}	2.42(7)–2.82(7)	H _{outer} ⋯H _{outer}	2.26(8)–3.01(8)2	H⋯H	2.55(4)–3.36(6)
	2.62		2.70		2.94
H _{outer} ⋯H _{center}	2.29(8)–2.79(9)	H _{outer} ⋯H _{center}	2.83(8)–3.30(8)		
	2.60		2.97		

Ba–H bonds in dimeric complexes: 2.47(5)–2.58(6) Å^[7,14] and is at the lower range for Ba–H distances in (HBaⁿ)₇ (2.55(3)–3.21(3) Å).^[15] While the Mg–H bonds between the five equatorial Mg²⁺ ions and the ten outer H[−] ligands (1.84(4)–2.09(7) Å) are within the range expected for Mg hydride complexes,^[4] those to the interstitial H[−] are much longer (2.25(6)–2.87(6) Å), however, not unprecedented in literature: Mg–H bond distances up to 2.63(3) Å have been reported.^[58]

It is more challenging to describe the geometry of the second Mg/Ba hydride cluster: Mg₄Ba₇H₁₃Nⁿ₉·(toluene)₂ (2); Figure 2. The structure of the cluster, which has no crystallographic symmetry, could be described as a central interstitial hydride ligand surrounded by a distorted tetrahedron of Ba²⁺ cations with Ba–H_{center} distances in the range 2.75(6)–2.88(6) Å. The Ba₄ tetrahedron is surrounded by 4 Mg²⁺ cations but the Mg–H_{center} distances are too long to be bonding interactions (2.95(6)–3.21(5) Å). The Mg₄Ba₄-framework resembles the geometry of a polyeder that is mathematically described as a snub “disphenoid”^[59] or “siamese dodecahedron” consisting of four Mg₂Ba and eight MgBa₂ faces, each with a μ₃-H[−] ligand (the

H_{outer} ligands). The periphery of this (Mg₄Ba₄H₁₃)³⁺ unit is stabilized by three barate BaNⁿ₃[−] anions and two neutral toluene ligands that cap Ba centers in η⁶-fashion. The Mg–H_{outer} (1.88(5)–2.09(6) Å) and Ba–H_{outer} (2.43(6)–2.74(6) Å) bonds are in the expected ranges.

The largest cluster, Mg₇Ba₁₂H₂₆Nⁿ₁₂ (3), is highly symmetric. It crystallizes in the trigonal spacegroup *R*-3, featuring a threefold inversion axis. The core of the cluster consists of a (MgH₆)⁴⁺ octahedron (Figure 3a). This unit with perfect H–Mg–H angles of 90° and 180° is enclosed by a (Ba₁₂H₂₀)⁴⁺ icosahedron consisting of 12 Ba²⁺ ions and 20 triangular Ba₃ faces that each contain a μ₃-H[−] ligand (Figure 3b). The twelve Ba²⁺ ions are adequately shielded by bonding to 6 MgNⁿ₂ units, each bridging between a pair of Ba²⁺ ions (Figure 3c). The formula for this cluster might therefore also be reformulated as [(MgH₆)(Ba₁₂H₂₀)(MgNⁿ₂)₆]. The Ba–H hydride (2.51(2)–2.83(3) Å) and Mg–H bond distances (1.87(3)–2.07(4) Å) are comparable to those of cluster 1 and 2.

The heterometallic Mg/Ba hydride clusters 1–3 are the first of their kind. During our investigation we never found

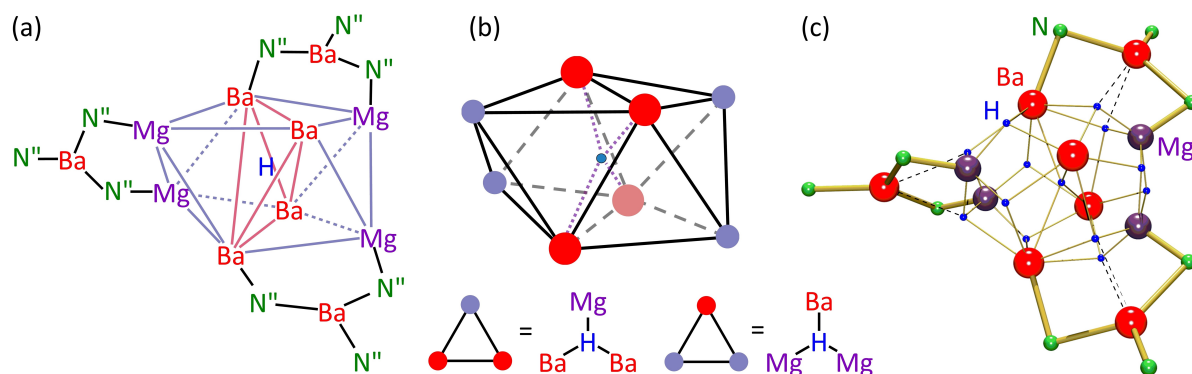


Figure 2. Crystal structure of Mg₄Ba₇H₁₃Nⁿ₉·(toluene)₂ (2); (a) Schematic representation. (b) The (Mg₄Ba₄H₁₃)³⁺ core of 2. (c) Structure of 2 with non-hydride H atoms and Me₃Si groups omitted for clarity.

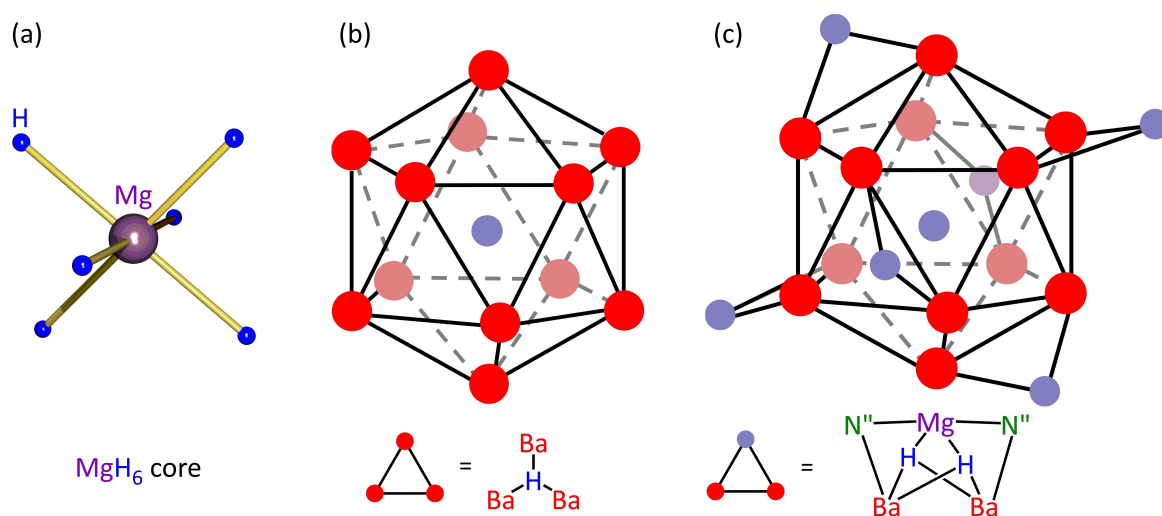


Figure 3. Crystal structure of Mg₇Ba₁₂H₂₆Nⁿ₁₂ (3). (a) The MgH₆⁴⁺ core. (b) Schematic representation of the surrounding Ba₁₂-dodecahedron. (c) Complete structure of 3.

precipitation of metal-pure metal hydride species, indicating that the interplay of the hard Lewis acidic Mg^{2+} ion and soft Ba^{2+} has a positive influence on the stability of mixed Ae metal hydride clusters.

Solution NMR studies

Complex $\text{Mg}_5\text{Ba}_4\text{H}_{11}\text{N}^{7-}(\text{benzene})_2$ (**1**) is sparingly soluble in benzene- d_6 . At room temperature three hydride singlet signals could be identified at 3.41, 3.36 and 3.29 ppm with an intensity ratio of 4:4:2, respectively. These chemical shifts fit for typical Mg hydride complexes which, with some exceptions, are generally in the 3.0–4.5 ppm range.^[4] They do not fit for Ba hydride complexes which feature hydride resonances at much lower field (range: 7.9–10.4 ppm).^[7,14,15] Their ratio of 4:4:2 fits well with the C_3 -symmetry of the cluster (Figure 1c). The fourth hydride signal, observed at 1.35 ppm, is assigned to the interstitial hydride ligand which is the most symmetric and least disturbed hydride ligand. Although this signal does not fit the general range for Mg or Ba hydride signals, its chemical shift is comparable to that for the interstitial hydride in the larger cluster $[(\text{para})_3\text{Mg}_8\text{H}_{10}]$ (para = a dianionic *para*-phenylene-bridged *bis*(β -diketimate) ligand).^[60] The central hydride ligand in this complex is linearly surrounded by two Mg^{2+} ions and shows a ^1H NMR resonance at 0.56 ppm. Although this value is considerably upfield from the $\delta = 3.0$ –4.6 ppm values reported for the α - MgH_2 phase, it fits for the β - MgH_2 phase ($\delta = 0.9$ ppm).^[61,62] The chemical shifts for the hydride ligands in **1** are clearly dominated by the Mg^{2+} cations and not by Ba^{2+} . High temperature NMR studies showed no coalescence of the hydride signals up to 80 °C. At higher temperatures decomposition by formation of HD is observed which was attributed to deprotonation of toluene- d_8 by the H^- ligand, a process that already slowly starts at 50 °C. The lack of coalescence at higher temperature demonstrates that the cluster **1** is very robust. It also shows that the symmetry-breaking BaN^{7+} cations, attached to the outside of the cluster, cannot wander freely over the cluster surface.

The complexes $\text{Mg}_4\text{Ba}_7\text{H}_{13}\text{N}^{9-}(\text{solvent})_2$ (**2**, solvent = benzene or toluene) are, once crystallized, poorly soluble in aromatic solvents. The ^1H NMR in benzene- d_6 shows five hydride signals at 5.45, 5.44, 4.65, 4.42 and 3.82 ppm in a ratio of 4:4:2:2:1. In agreement with the mixed-metal character of the cluster, these chemical shift values are too high for a typical Mg–H resonance and too low in comparison with typical Ba–H resonances. A two-dimensional $^1\text{H}, ^1\text{H}$ -COSY spectrum (Figure S10) revealed correlation between the two signals of highest intensity (4) and the smallest signal (1). While the latter high-field signal at 3.82 ppm is assigned to the interstitial hydride, the two most intense hydride signals with the highest chemical shifts (5.44 and 5.45 ppm) are assigned to the eight hydrides sitting on Ba_2Mg -faces (which are different due to the symmetry breaking BaN_3^{7-} anions and η^6 -toluene ligands). The two remaining hydride resonances at 4.42 and 4.65 ppm, both with intensity 2, are assigned to hydrides on the four Mg_2Ba -faces. It should be noted that chemical shifts for hydrides on

the Ba-rich Ba_2Mg -faces are higher than those for hydrides at Mg-rich Mg_2Ba -faces. This is in agreement with the heavy metal effect which causes hydrides with close metal contacts to shift downfield (the heavier the metal, the larger the downfield shift).^[63,64]

Theoretical considerations

Complexes **1**–**3** have been analyzed by DFT methods at the B3PW91/def2tzvp level using core potentials at Ba. For simplicity the $(\text{Me}_3\text{Si})_2\text{N}^-$ anions have been replaced by Me_2N^- anions (abbreviated as N^*). These model clusters, which are indicated as **1***, **2*** and **3***, resemble the experimentally determined crystal structures reasonably well (Table S2). The NPA charges for Mg, Ba and the hydride ligands in **1***–**3*** are all comparable and in a narrow range: Mg +1.58/+1.63, Ba +1.70/+1.79 and H -0.80 / -0.88 (Table S3). These values indicate highly ionic bonds. The NPA charges for Mg in **1***–**3*** compare well to those in recently reported Mg hydride dimer complexes stabilized by the $(\text{Me}_3\text{Si})_2\text{N}^-$ anion and neutral Lewis bases: Mg +1.63/+1.67.^[65] Charges on the hydrides in the latter Mg hydride dimer (H -0.79) are at the lower end of those in **1***–**3***. The NPA charges for Ba in **1***–**3*** compare well to those in the related $(\text{HBaN}^*)_7$ cluster (F in Scheme 1) which vary from +1.68 to +1.77. Charges on the hydrides in $(\text{HBaN}^*)_7$ range from -0.83 to -0.86 and are at the higher boundary of those in **1***–**3***.

Atoms-in-molecules (AIM) analysis of cluster **1*** shows bond paths between the interstitial hydride and the two axial Ba^{2+} ions with an electron density in the bond-critical-points (bcp's) of $0.162 \text{ e} \cdot \text{\AA}^{-3}$. These Ba–H bonds are much stronger than those between Ba and the five outer hydrides in the periphery of the cluster (0.132 – $0.136 \text{ e} \cdot \text{\AA}^{-3}$). Bonding between the interstitial hydride and the five Mg^{2+} ions in the equatorial plane is indicated by bcp's but is much weaker ($0.103 \text{ e} \cdot \text{\AA}^{-3}$) due to long Mg–H distances (*vide supra*). Electron densities in bcp's on Mg–H bonds within the $(\text{MgH}_2)_5$ belt are up to twice as high (0.158 – $0.209 \text{ e} \cdot \text{\AA}^{-3}$). These values are in favor of describing **1*** as a central $(\text{C}_6\text{H}_6)\text{Ba}(\text{H})\text{Ba}(\text{C}_6\text{H}_6)^{3+}$ spindle surrounded by a neutral $(\text{MgH}_2)_5$ -belt. The most pronounced bcp's ($0.232 \text{ e} \cdot \text{\AA}^{-3}$) were found between the two barate $\text{BaN}^*_3^-$ motifs and the hydride core Mg_5H_{10} belt.

The interstitial hydride in complex **2*** shows only bcp's to the four neighboring Ba^{2+} ions (0.066 – $0.111 \text{ e} \cdot \text{\AA}^{-3}$) and not to the more remote Mg^{2+} ions. This observation is in accordance with the very long distance of the Mg^{2+} to central hydride in **2** ($2.95(6)$ – $3.21(5) \text{ \AA}$ [Avg. 3.07 \AA]) or **2*** (2.91 – 3.04 \AA [Avg. 2.97]). There are, however, bond paths between Mg^{2+} and neighboring H_{outer} ligands with electron densities (0.180 – $0.213 \text{ e} \cdot \text{\AA}^{-3}$) that are considerably higher than the Ba– H_{outer} bond paths (0.103 – $0.174 \text{ e} \cdot \text{\AA}^{-3}$). The most pronounced metal hydride interaction was again found between the three barate $\text{BaN}^*_3^-$ motifs interacting with one close hydride ligand ($0.213 \text{ e} \cdot \text{\AA}^{-3}$).

AIM analysis shows that the Mg–H and Ba–H bonding in **3*** is similar to that in **1*** and **2***. The electron densities in Ba–H

bcp's are in the $0.069\text{--}0.147\text{ e}\cdot\text{\AA}^{-3}$ range while those in Mg–H bcp's indicate somewhat stronger bonding ($0.174\text{--}0.209\text{ e}\cdot\text{\AA}^{-3}$).

Apart from metal-hydride bond paths, we noted in all three clusters unusual bcp's between two hydride ligands (Figure 4). In complexes **1*** and **2*** these unexpected $\text{H}\cdots\text{H}^-$ interactions are observed between the interstitial hydrides and the H_{outer} ligands (**1***: $0.086\text{--}0.127\text{ e}\cdot\text{\AA}^{-3}$, **2***: $0.051\text{--}0.082\text{ e}\cdot\text{\AA}^{-3}$). Bonding between H_{outer} ligands is in both complexes somewhat more pronounced (**1***: $0.132\text{ e}\cdot\text{\AA}^{-3}$, **2***: $0.139\text{--}0.140\text{ e}\cdot\text{\AA}^{-3}$). In cluster **3***, bcp's were noted between hydrides of the formal core unit $[\text{MgH}_6]^{4-}$ and twelve H_{outer} ligands located in the $\text{Ba}_{12}\text{H}_{20}$ shell ($0.061\text{--}0.073\text{ e}\cdot\text{\AA}^{-3}$). Although the electron densities in the bcp's are low they are significant. Electron densities in the bcp's for $\text{H}\cdots\text{H}^-$ interactions in **1*–3*** ($0.05\text{--}0.14\text{ e}\cdot\text{\AA}^{-3}$), are comparable to those in a recently reported dodecanuclear Ca hydride cluster ($0.10\text{--}0.13\text{ e}\cdot\text{\AA}^{-3}$)^[10] and considerably larger than those found in a tetranuclear Mg hydride cluster ($0.047\text{ e}\cdot\text{\AA}^{-3}$, $\text{H}\cdots\text{H} = 3.106\text{ \AA}$).^[66] It appears that hydride-hydride interaction is a common feature in larger alkaline earth metal hydride aggregates. Shorter $\text{H}\cdots\text{H}^-$ distances generally result in high electron densities in the corresponding bcp's.

Catalytic hydrogenation

Cooperative effects between metal complexes from the first and second main groups are widespread in literature.^[38–41] The combination KH/AeN''_2 ($\text{Ae}=\text{Mg, Ca}$) was recently put forward as a hydrogenation catalyst for activated (conjugated) alkenes, terminal unactivated alkenes or cyclic internal alkenes.^[67] Screening all alkali metals, mixtures of MN'' ($\text{M}=\text{Li, Na, K, Rb, Cs}$) and MgN''_2 were shown to be catalysts for transferring hydrogen from 1,4-cyclohexadiene to either $\text{Ph}_2\text{C}=\text{CH}_2$ or $\text{Ph}(\text{H})\text{C}=\text{CH}_2$.^[37] It is notable that each component alone was not active in this catalytic transformation. Herein we present first

studies on mixed Ae metal hydride catalysts in which we combine a hard metal (Mg) with a soft metal (Ba).

For evaluation of possible cooperative effects between Mg and Ba, catalytic alkene hydrogenation was not only studied with the $\text{MgN}''_2/\text{BaN}''_2$ mixture but also with the metal-pure precursors MgN''_2 and BaN''_2 alone. Reaction conditions were adapted from previously established hydrogenation protocols using the AeN''_2 precursors ($120\text{ }^\circ\text{C}$, 6 bar H_2).^[20,21,23] In order to observe activity for the least active catalyst MgN''_2 , high catalyst loadings of 20 mol% were used. In order to compare results, for the $\text{MgN}''_2/\text{BaN}''_2$ mixture 10 mol% of each has been used which equals 20 mol% total metal content. Although for consistency the metal-pure BaN''_2 catalyst was also used in 20 mol% quantity in most cases, it must be realized that for this highly active catalyst the loadings can be reduced significantly.^[20,21,23] Part of the catalytic runs were repeated with the mixed Mg/Ba cluster **1** in which case catalyst loadings of 1.8 mol% were used. Considering the cluster contains 11 hydrides, this converts to circa 20 mol% based on hydride content.

Table 2 shows that MgN''_2 is generally fully inactive in alkene hydrogenation. A similar observation was made for transfer hydrogenation of alkenes.^[37] Also in alkyne hydrogenation no activity was found (entry 6) but, as we reported previously,^[20] MgN''_2 is catalytically active in imine hydrogenation (entries 7–12).

In contrast to the poor activity of MgN''_2 in alkene hydrogenation, the mixed-metal system $\text{MgN}''_2/\text{BaN}''_2$ can reduce terminal alkenes like 1-hexene (entry 1), however, with low activity. Precatalyst BaN''_2 alone showed under similar conditions full conversion of 1-hexene but considerable isomerization to 2-hexene was found as a side-reaction.^[21] As internal alkenes are much harder to reduce than terminal alkenes, no further hydrogenation to *n*-hexane was observed. The double bonds in vinyltrimethylsilane and 4-vinyl-cyclohexene cannot be isomerized and show higher conversions (entries 2–3). The reluctance

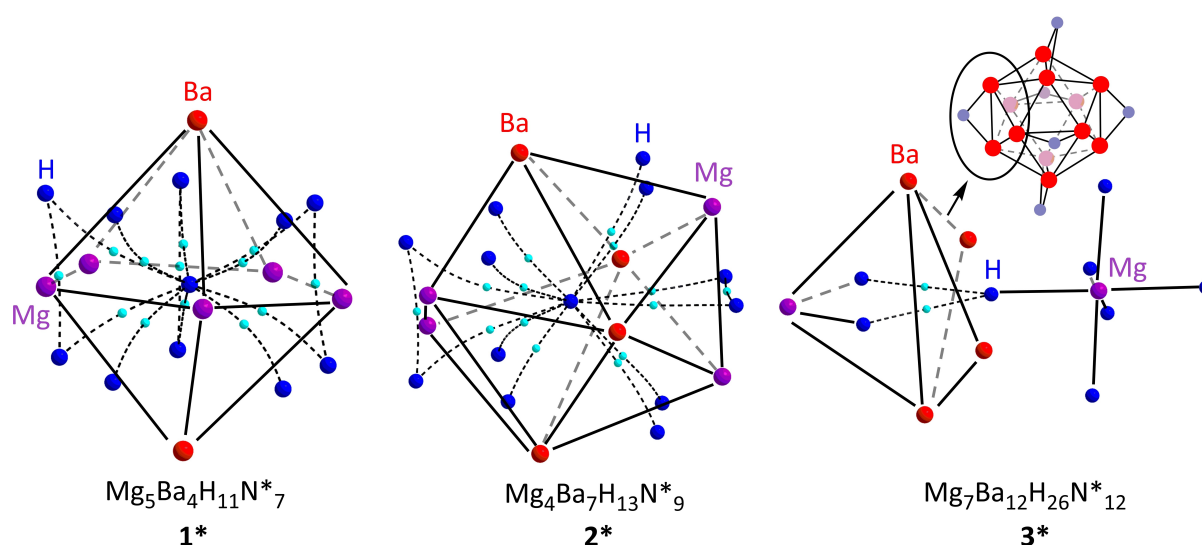
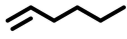
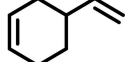
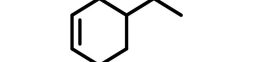
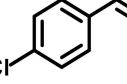
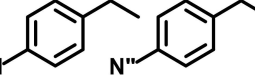
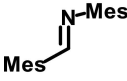
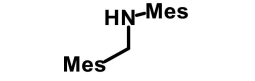
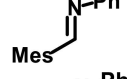
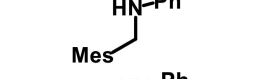
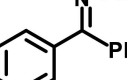
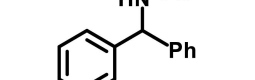
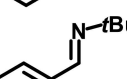
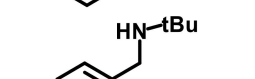
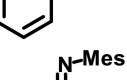
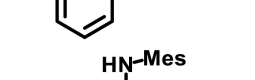
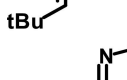
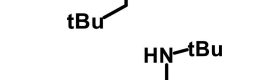


Figure 4. Atoms-in-molecules (AIM) representation of the metal hydride cores in **1*–3*** exclusively showing the unusual hydride-hydride bond paths and bond-critical-points (light-blue). For the highly symmetric complex **3*** only the asymmetric unit is shown, representing the whole complex.

Table 2. Catalytic alkene, alkyne and imine hydrogenation (20 mol% catalyst, substrate concentration = 0.11 M, 120 °C, 6 bar H₂). Reactions with **1** (1.8 mol% catalyst, substrate concentration = 0.28 M, 120 °C, 6 bar H₂). Conversions determined by GC-MS analysis (average of at least three runs).

Entry	Substrate	t [h]	Product(s)	MgN ^{II} ₂ [%]	Mg/Ba ^a [%]	BaN ^{II} ₂ [%]	1 [%]
1		24		trace	27/2	42/58 ^[b]	–
2		2		3	88	99 ^[c]	88
3		24		2	64	73 ^[b]	–
4		24		93/5/3/0	0/0/67/33	0/0/43/57	0/0/63/27
5		24		trace	1/23	4/23	–
6		1		1/0	100/0	100/0	79/20
7		2		75	94	100	–
8		2		79	59	96	47
9		2		56	91	99	76
10		1		85	100	100	100
11		2		43	77	93	–
12		2		0	100	100	100

[a] MgN^{II}₂/BaN^{II}₂ ratio 1 : 1. In this case 10 mol% of each, MgN^{II}₂ and BaN^{II}₂, was used. The total metal amount is 20 mol%, [b] 10 mol% catalyst loading,^[21] [c] 10 mol% catalyst loading @ 0.5 h reaction time.^[21]

to hydrogenate internal alkenes is supported by the selective hydrogenation of the vinyl group in 4-vinyl-cyclohexene. Exceptions are the double bonds in norbornadiene which are activated for reduction but also give nortricyclene as a side-product (entry 4). Like for BaN^{II}₂, conversion of *p*-Cl-styrene is accompanied by nucleophilic aromatic substitution (entry 5) but diphenylacetylene could be fully reduced by the MgN^{II}₂/BaN^{II}₂ system (entry 6). Various imines (aldimine or ketimine) could be hydrogenated with the MgN^{II}₂/BaN^{II}₂ combination (entries 7–12).

It seems that the presence of Ba is essential for alkene and alkyne hydrogenation whereas for imine hydrogenation MgN^{II}₂ already showed good activity. This may be explained by activation of the imine substrate by Mg⋯N(R)=C(H)R' coordination, a complex in which a hard Mg cation combines with a hard N Lewis base. The fact that MgN^{II}₂ alone does not perform

in alkene hydrogenation is likely related to the lower ionicity of the Mg–H bond (*cf.* the Ba–H bond) and its inherently lower reactivity. Additionally, it also could be due to poor coordination of soft alkene ligands to hard Mg²⁺ cations. Activation of unsaturated substrates by Ae metal ions has been shown essential in catalysis.^[68,69] Isolation of unsupported Mg⋯alkene (or alkyne and arene) complexes so far has only been achieved with highly Lewis acidic cationic Mg complexes which are free of stabilizing Lewis bases.^[70–76] It has been found that the heavier softer Ae metals Ca, Sr and Ba are superior in activating soft unsaturated substrates.^[11,29,33] This is also supported by the crystal structures of **1** and **2** in which the arene ligands coordinate exclusively to the larger Ba metal and not to Mg and explains why the presence of Ba is crucial for alkene and alkyne activation.

With few exceptions the activity of the mixed-metal catalyst generally lies between that of its individual components. These results demonstrate that, although there are certainly differences in activity between the three catalysts, mixing Mg and Ba does not have an additional advantage over using Ba alone. In order to understand the nature of the mixed catalyst $\text{MgN}''_2/\text{BaN}''_2$, a solution of this combination in C_6D_6 was pressurized with H_2 (6 bar) and heated to 80°C (6 h). While a similar reaction of CaN''_2 with H_2 led to formation of undefined $\text{Ca}_x\text{H}_y\text{N}''_z$ clusters with MW's up to $7500\text{ g}\cdot\text{mol}^{-1}$,^[20] the $\text{MgN}''_2/\text{BaN}''_2$ mixture reacted with H_2 to give primarily $\text{Mg}_5\text{Ba}_4\text{H}_{11}\text{N}''_7\cdot(\text{benzene})_2$ (1) together with minor quantities of unknown hydride complexes, indicated by ^1H NMR signals in the 5.0–5.3 ppm region (Figure S42–43). The formation of 1 was further confirmed by its crystallization from this solution. The clusters 1–3 are therefore valid models for intermediates that could form during catalytic hydrogenation with $\text{MgN}''_2/\text{BaN}''_2$. Indeed, cluster 1 has been successfully used as a hydrogenation catalyst (Table 2). In all cases the catalytic activity of 1 is comparable to that of the $\text{MgN}''_2/\text{BaN}''_2$ mixture, supporting the idea that these mixed metal Mg/Ba hydride clusters are the catalytically active species.

Conclusions

Reaction of a mixture of MgN''_2 and BaN''_2 with PhSiH_3 resulted in the formation of three unique heterometallic Mg/Ba hydride clusters $\text{Mg}_5\text{Ba}_4\text{H}_{11}\text{N}''_7\cdot(\text{benzene})_2$ (1), $\text{Mg}_4\text{Ba}_7\text{H}_{13}\text{N}''_9\cdot(\text{solvent})_2$ (2) (solvent = benzene or toluene) and $\text{Mg}_7\text{Ba}_{12}\text{H}_{26}\text{N}''_{12}$ (3). The educt composition influences the Mg/Ba ratio in the metal hydride clusters which become richer in Ba with lower $\text{MgN}''_2/\text{BaN}''_2$ ratios. Cluster composition can also be influenced by temperature. While cluster 1 is thermally stable, cluster 2 is thermolabile and forms at higher temperatures the larger Mg/Ba hydride cluster $\text{Mg}_7\text{Ba}_{12}\text{H}_{26}\text{N}''_{12}$ (3) which is completely insoluble in aromatic solvents. These clusters, which can all be prepared phase-pure, are among the first examples of well-characterized Ae heterobimetallic hydrides. Under no circumstances were homometallic clusters isolated, indicating that the mixing of Mg^{2+} and Ba^{2+} cations has a positive influence on cluster stability.

While the insoluble cluster 3 could not be studied in solution, the solid state structures of 1 and 2 are retained when dissolved in aromatic solvents. The high symmetry of the $\text{Mg}_x\text{Ba}_y\text{H}_z$ cores found in the solid state structures of 1 and 2 is broken by coordination of BaN'' units in the periphery. This makes the hydride ligands in the core inequivalent, leading to several hydride resonances in the ^1H NMR spectra. It is surprising that the clusters 1 and 2 do not show dynamical ligand exchange processes that are typical for *s*-block metal compounds, also not at higher temperature ($+80^\circ\text{C}$). The chemical shifts for the hydride ligands in 1 and 2 range from 1.35 to 5.45 ppm, and should be regarded more typical for Mg–H resonances (0.55–6.78 ppm) than for Ba–H resonances (7.9–10.4 ppm).

DFT calculation on model system for 1–3 reproduced their structures reasonably well. AIM analysis showed bcp's between

the metals and hydride ligands. The electron density on the Mg–H bond paths is generally higher than that on Ba–H bond paths which is due to higher covalency in the Mg–H bond. This is confirmed by calculation of the NPA charges which are higher for Ba^{2+} when compared to Mg^{2+} . All clusters also show unusual $\text{H}^-\cdots\text{H}^-$ bond paths but the electron densities in their bcp's are generally low ($0.05\text{--}0.14\text{ e}\cdot\text{\AA}^{-3}$).

The activity of the mixture $\text{MgN}''_2/\text{BaN}''_2$ in hydrogenation catalysis was compared to that of the metal pure catalysts MgN''_2 and BaN''_2 . A solution of the $\text{MgN}''_2/\text{BaN}''_2$ mixture in benzene reacts with H_2 to give primarily $\text{Mg}_5\text{Ba}_4\text{H}_{11}\text{N}''_7\cdot(\text{benzene})_2$ (1). The MgN''_2 (pre)catalyst is not active in alkene or alkyne hydrogenation but is effective in imine hydrogenation. The $\text{MgN}''_2/\text{BaN}''_2$ mixture was found to be active in alkene, alkyne and imine hydrogenation, however, the activities are in general lower or equal to that of BaN''_2 . This clearly shows that, although imine hydrogenation can also be performed with Mg-based catalysts, for alkene and alkyne hydrogenation the presence of Ba is crucial. This may be explained by the HSAB concept in which hard Lewis acids (Mg^{2+}) bind and activate hard Lewis bases (imines) whereas soft Lewis bases (alkenes and alkynes) need the softer Ba^{2+} for activation. A combination of hard (Mg^{2+}) and soft (Ba^{2+}) does, at least in catalytic hydrogenation, not provide additional benefits. This is mainly due to the very high performance of metal-pure Ba catalysts.

Experimental Section

General Experimental Procedures

All experiments were conducted in dry glassware under an inert nitrogen atmosphere by applying standard Schlenk techniques or gloveboxes (MBraun) using freshly dried and degassed solvents. Benzene, toluene, pentane and hexane were degassed with nitrogen, dried over activated aluminum oxide (Innovative Technology, Pure Solv 400–4-MD, Solvent Purification System) and then stored under inert atmosphere. Deuterated benzene (C_6D_6 ; 99.6 + %D) and toluene- d_8 (99.6 + %D) were purchased from Deutero GmbH and Euriso-top, degassed and dried over molecular sieves (3 Å). Following reagents were obtained commercially and dried over molecular sieves (3 Å): PhSiH_3 (Alfa Aesar, 97%), cyclohexene (Fluka, 99%), 1-hexene (Acros Organics, 97%), 4-vinyl-1-cyclohexene (TCI Chemicals, > 95%), 4-chloro-styrene (TCI, > 98%), norbornadiene (Sigma-Aldrich, 98%), $\text{Ph}(\text{H})\text{C}=\text{NtBu}$ (Sigma-Aldrich, 97%). Diphenylacetylene (Sigma-Aldrich, 98%) was dried under high vacuum for two days at 60°C . Following substrates were synthesized according to literature procedures: *p*-MeO– $\text{PhC}(\text{H})=\text{NtBu}$,^[77] $\text{Ph}(\text{Ph})\text{C}=\text{N}(\text{Ph})$,^[78] $t\text{Bu}(\text{H})\text{C}=\text{N}(\text{Mes})$,^[79] $\text{Mes}(\text{H})\text{C}=\text{N}(\text{Mes})$,^[80] $\text{Mes}(\text{H})\text{C}=\text{N}(\text{Ph})$.^[80] The following compounds were synthesized according to literature procedures: $\text{Mg}[\text{N}(\text{SiMe}_3)_2]_2$ (MgN''_2) and $\text{Ba}[\text{N}(\text{SiMe}_3)_2]_2$ (BaN''_2).^[81] NMR spectra were measured on Bruker Avance III HD 400 MHz and Bruker Avance III HD 600 MHz spectrometers. Chemical shifts (δ) are denoted in ppm (parts per million), coupling constants in Hz (Hertz). For describing signal multiplicities common abbreviations are used: s (singlet) and m (multiplet). Spectra were referenced to the solvent residual signal. Elemental analysis was performed with an Hekatech Eurovector EA3000 analyzer. All crystal structures have been measured on a SuperNova (Agilent) diffractometer with dual Cu and Mo microfocus sources and an Atlas S2 detector. Crystallo-

graphic data have been deposited with the Cambridge Crystallographic Data Centre as supplementary publication numbers: CCDC 2096695 (1), 2096646 (2) and 2096696 (3).

GC-MS measurements were performed on a Thermo Scientific™ Trace™ 1310 gas chromatography system (carrier gas Helium) with detection by a Thermo Scientific™ ISQ™ LT Single Quadrupole mass spectrometer. A Phenomenex® Zebtron™ ZB-5 GC column of the dimensions 0.25 mm×30 m with a film thickness of 0.25 μm or a Thermo Scientific™ TraceGOLD™ TG-5SiIMS GC Column of the dimensions 0.25 mm×30 m with a film thickness of 0.25 μm was used. The samples (1 μL) were injected with an Instant Connect-SSL Module in the split mode (injector temperature: 280 °C). Temperature programs were started at 40 °C followed by heating ramps, optimized for the separation problem, until 280°. Baseline separation of each analyte was achieved by choosing the different temperature programs. The molecular identities were confirmed by comparison with entries in the NIST/EPA/NIH mass spectral library (v2.2, built June 10 2014) or by comparing to authentic samples.

Synthesis of Mg₅Ba₄H₁₁N₇·(benzene)₂ (1). A mixture of BaN₂ (50.0 mg, 0.11 mmol) and MgN₂ (47.1 mg, 0.14 mmol) was suspended in 1.5 mL of benzene (the chosen Mg/Ba ratio represents that in 1). The mixture was shortly heated to reflux to dissolve all solids. PhSiH₃ (32.5 mg, 0.30 mmol, 37.0 μL) was added followed by vigorous shaking of the solution. Colorless crystals formed over the next two days. The crystals were isolated and dried at 60 °C under vacuum to afford 25 mg of pure Mg₅Ba₄H₁₁N₇·(benzene)₂ (25 mg, 0.013 mmol, 46% based on BaN₂). Yield was calculated on the basis that four eq. of BaN₂ are needed to form one eq. of Mg₅Ba₄H₁₁N₇·(benzene)₂ complex. ¹H NMR (600.13 MHz, benzene-*d*₆, 298 K): δ = 3.41 (s, 4H, H), 3.36 (s, 4H, H), 3.29 (s, 2H, H), 1.35 (s, 1H, H), 0.50 (s, 18H, Si[CH₃]₃), 0.49 (s, 72H, Si[CH₃]₃), 0.43 (s, 36H, Si[CH₃]₃) ppm. ¹³C{¹H} NMR (150.92 MHz, benzene-*d*₆, 298 K): δ = 6.76 (Si[CH₃]₃), 6.68 (Si[CH₃]₃), 6.33 (Si[CH₃]₃), 6.25 (Si[CH₃]₃) ppm. ²⁹Si NMR (119.22 MHz, benzene-*d*₆, 298 K) δ = -4.41 (Si[CH₃]₃), -5.07 (Si[CH₃]₃), -8.62 (Si[CH₃]₃), -16.49 (Si[CH₃]₃) ppm. FT-IR (ATR, pure): $\tilde{\nu}$ = 2943 (m), 2891 (w), 1477 (w), 1245 (m), 1107 (w), 1000 (m), 933 (m), 814 (s), 751 (m), 699 (m), 661 (m), 634 (m), 603 (m), 552 (m), 429 (w), 415 (w) cm⁻¹. Decomposition point: 210–212 °C. Elemental analysis calculated for C₆₀H₁₅₅Ba₄Mg₅N₇Si₁₄ = Mg₅Ba₄H₁₁N₇·(benzene)₃ (MW 2038.95 g/mol) (isolated without drying step but after washing with pentane. Residual pentane was allowed to evaporate into the glovebox atmosphere): C 35.34, H 7.66, N 4.81; Found: C 35.29, H 7.58, N 4.66.

Synthesis of Mg₄Ba₇H₁₃N₉·(benzene)₂ (2). A mixture of BaN₂ (232 mg, 0.506 mmol) and MgN₂ (100 mg, 0.290 mmol) was suspended in 3 mL of benzene (the chosen Mg/Ba ratio represents that in 2). The mixture was shortly heated to reflux to dissolve all solids. PhSiH₃ (102 mg, 0.943 mmol, 116 μL) was diluted in benzene (1.8 mL) and added dropwise to the stirring solution. The brownish solution was stirred for 1.5 h at room temperature. The formation of a white precipitate was observed. The reaction mixture was allowed to settle and the solution was decanted. The remaining white solid was washed with pentane (3×1.5 mL) and dried under vacuum at 60 °C to obtain 66 mg (0.025 mmol) of pure Mg₄Ba₇H₁₃N₉·(benzene)₂ in 34% yield, based on BaN₂. Yield was calculated on the basis that seven eq. of BaN₂ are needed to form one eq. of Mg₄Ba₇H₁₃N₉·(benzene)₂ complex. The toluene adduct could be isolated by repeating the procedure in toluene. Clear colorless crystals of Mg₄Ba₇H₁₃N₉·(toluene)₂×toluene were isolated from a saturated toluene solution after one week at room temperature. The compound is poorly soluble in benzene-*d*₆. ¹H NMR (600.13 MHz, benzene-*d*₆, 298 K): δ = 5.45 (s, 4H, H), 5.44 (s, 4H, H), 4.65 (s, 2H, H), 4.42 (s, 2H, H), 3.82 (s, 1H, H), 0.52–0.45 (m, 90H, Si[CH₃]₃), 0.43 (m, 72H, Si[CH₃]₃) ppm. ¹³C{¹H} NMR (150.92 MHz, benzene-*d*₆, 298 K): δ = 7.27 (Si[CH₃]₃), 7.05 (Si[CH₃]₃), 6.59 (Si[CH₃]₃),

6.37 (Si[CH₃]₃), 6.20 (Si[CH₃]₃) ppm. ²⁹Si NMR (119.22 MHz, benzene-*d*₆, 298 K) δ = -4.60 (Si[CH₃]₃), -5.58 (Si[CH₃]₃), -12.07 (Si[CH₃]₃), -16.58 (Si[CH₃]₃), -17.31 (Si[CH₃]₃) ppm. FT-IR (ATR, pure): $\tilde{\nu}$ = 2942 (m), 2890 (w), 1477 (w), 1244 (m), 1142 (w), 1033 (m), 999 (m), 951 (s), 861 (m), 812 (s), 755 (s), 699 (s), 660 (s), 602 (m), 575 (m), 445 (w), 424 (w) cm⁻¹. Decomposition point: 240–241 °C. Elemental analysis Calculated for C₆₆H₁₈₇Ba₇Mg₄N₉Si₁₈: Mg₄Ba₇H₁₃N₉·(benzene)₂ (MW 2671.32 g/mol): C 29.68, H 7.06, N 4.72; Found: C 29.85, H 7.05, N 4.36.

Synthesis of Mg₇Ba₁₂H₂₆N₁₂ (3). A mixture of BaN₂ (60.0 mg, 0.131 mmol) and MgN₂ (26.4 mg, 0.076 mmol) was suspended in 1.8 mL of hexane in a 20 mL vial (the chosen Mg/Ba ratio represents that in 3). The mixture was shortly heated to reflux to dissolve all solids. PhSiH₃ (30.7 mg, 0.284 mmol, 35 μL) was diluted in hexane (200 μL) and added dropwise to the stirring solution. The solution turned yellowish and was transferred to an NMR tube. The reaction mixture was heated to 70 °C for 12 h to obtain clear, colorless crystals. The crystals (11.4 mg) were washed with hexane (3×1 mL) and dried shortly under vacuum. The complex shows no solubility in cyclohexane-*d*₁₂, hot benzene-*d*₆, benzene-*d*₆/THF-*d*₈ mixture or THF-*d*₆. Its identity was repeatedly confirmed by cell parameter check using X-ray diffractometry. FT-IR (ATR, pure): $\tilde{\nu}$ = 2948 (m), 2929 (m), 1434 (w), 1245 (m), 1058 (w), 964 (s), 869 (s), 826 (s), 741 (s), 691 (m), 657 (m), 612 (m), 601 (m), 459 (m) cm⁻¹. Decomposition point: 278–279 °C. Elemental analysis Calculated for C₇₂H₂₄₂Ba₁₂Mg₇N₁₂Si₂₄ (MW 3768.91): C 22.95, H 6.47, N 4.46; Found: C 22.27, H 6.14, N 3.43.

Catalytic hydrogenation with MgN₂ and BaN₂ mixtures. The catalyst, MgN₂ (0.022 mmol, 20 mol%), BaN₂ (0.022 mmol, 20 mol%) or the mixture MgN₂/BaN₂ (0.011 mmol of each), was dissolved in dry toluene (1.0 ml) in a steel autoclave (15 ml) under an atmosphere of nitrogen and the substrate (0.110 mmol) was added to the solution. The tightly sealed autoclave was applied with hydrogen pressure (6 bar), stirred and quickly heated to the desired temperature (120 °C) in a heating block. The conversion after the given time was determined by subsequent GC-MS analysis of the quenched reaction mixture.

Catalytic hydrogenation with Mg₅Ba₄H₁₁N₇·(benzene)₂ (1). Complex 1 (10.0 mg, 5.1 μmol, 1.8 mol%) was dissolved in dry toluene (1.0 ml) in a steel autoclave (15 ml) under an atmosphere of pure nitrogen and the substrate (0.28 mmol) was added to the solution. The tightly sealed autoclave was applied with hydrogen pressure (6 bar), stirred and heated to the desired temperature (120 °C) quickly in a heating block. The conversion after the given time was determined by subsequent GC-MS analysis of the quenched reaction mixture. [NOTE: Complex concentration appears to be low at 1.8 mol%, however, normalized to 11 hydrides per complex, the total concentration of hydrides would be ≈ 20 mol%]

Supporting Information

¹H, ¹³C, ²⁹Si NMR, DOSY and variable temperature NMR spectra for complexes 1 and 2, ATR-IR-spectra are provided for 1-3. ¹H NMR monitoring of catalytic reactions, crystallographic details including ORTEP plots, details for the DFT calculations including XYZ-files.

Acknowledgement

We acknowledge C. Wronna and A. Roth for CHN analyses and Dr. C. Färber and J. Schmidt for assistance with NMR analyses. We thank the Deutsche Forschungsgemeinschaft for funding (HA 3218/9-1). Open Access funding enabled and organized by Projekt DEAL.

Conflict of Interest

The authors declare no conflict of interest.

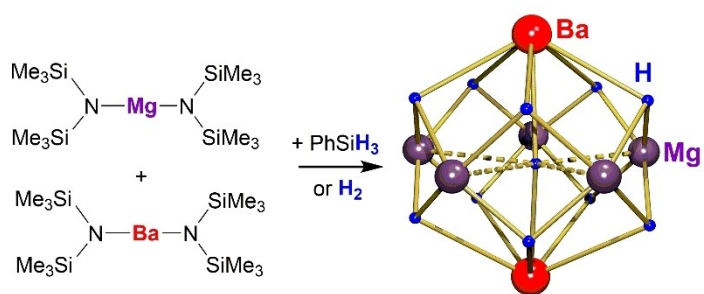
Keywords: alkaline earth metal · hydride · heterometallic · catalysis · DFT calculations

- [1] S. Harder, J. Brettar, *Angew. Chem. Int. Ed.* **2006**, *45*, 3474–3478; *Angew. Chem.* **2006**, *118*, 3554–3558.
- [2] S. Harder, *Chem. Commun.* **2012**, *48*, 11165.
- [3] L. Fohlmeister, A. Stasch, *Aust. J. Chem.* **2015**, *68*, 1190–1201.
- [4] D. Mukherjee, J. Okuda, *Angew. Chem. Int. Ed.* **2018**, *57*, 1458–1473; *Angew. Chem.* **2018**, *130*, 1472–1488.
- [5] D. Mukherjee, D. Schuhknecht, J. Okuda, *Angew. Chem. Int. Ed.* **2018**, *57*, 9590–9602; *Angew. Chem.* **2018**, *130*, 9736–9749.
- [6] S. P. Green, C. Jones, A. Stasch, *Angew. Chem. Int. Ed.* **2008**, *47*, 9079–9083; *Angew. Chem.* **2008**, *120*, 9219–9223.
- [7] X. Shi, G. Qin, Y. Wang, L. Zhao, Z. Liu, J. Cheng, *Angew. Chem. Int. Ed.* **2019**, *58*, 4356–4360; *Angew. Chem.* **2019**, *131*, 4400–4404.
- [8] D. Mukherjee, T. Höllerhage, V. Leich, T. P. Spaniol, U. Englert, L. Maron, J. Okuda, *J. Am. Chem. Soc.* **2018**, *140*, 3403–3411.
- [9] C. N. De Bruin-Dickason, T. Sutcliffe, C. Alvarez Lamsfus, G. B. Deacon, L. Maron, C. Jones, *Chem. Commun.* **2018**, *54*, 786–789.
- [10] J. Martin, J. Eyselien, J. Langer, H. Elsen, S. Harder, *Chem. Commun.* **2020**, *56*, 9178–9181.
- [11] B. Rösch, T. X. Gentner, H. Elsen, C. A. Fischer, J. Langer, M. Wiesinger, S. Harder, *Angew. Chem. Int. Ed.* **2019**, *58*, 5396–5401; *Angew. Chem.* **2019**, *131*, 5450–5455.
- [12] B. Maitland, M. Wiesinger, J. Langer, G. Ballmann, J. Pahl, H. Elsen, C. Färber, S. Harder, *Angew. Chem. Int. Ed.* **2017**, *56*, 11880.
- [13] T. Höllerhage, A. Carpentier, T. P. Spaniol, L. Maron, U. Englert, J. Okuda, *Chem. Commun.* **2021**, *57*, 6316–6319.
- [14] X. Shi, C. Hou, C. Zhou, Y. Song, J. Cheng, *Angew. Chem. Int. Ed.* **2017**, *56*, 16650–16653; *Angew. Chem.* **2017**, *129*, 16877–16880.
- [15] M. Wiesinger, B. Maitland, C. Färber, G. Ballmann, C. Fischer, H. Elsen, S. Harder, *Angew. Chem. Int. Ed.* **2017**, *56*, 16654–16659; *Angew. Chem.* **2017**, *129*, 16881–16886.
- [16] J. Spielmann, S. Harder, *Chem. A Eur. J.* **2007**, *13*, 8928–8938.
- [17] J. Spielmann, F. Buch, S. Harder, *Angew. Chem. Int. Ed.* **2008**, *47*, 9434–9438; *Angew. Chem.* **2008**, *120*, 9576–9580.
- [18] D. Schuhknecht, C. Lhotzky, T. P. Spaniol, L. Maron, J. Okuda, *Angew. Chem. Int. Ed.* **2017**, *56*, 12367–12371; *Angew. Chem.* **2017**, *129*, 12539–12543.
- [19] T. Höllerhage, D. Schuhknecht, A. Mistry, T. P. Spaniol, Y. Yang, L. Maron, J. Okuda, *Chem. A Eur. J.* **2021**, *27*, 3002–3007.
- [20] H. Bauer, M. Alonso, C. Färber, H. Elsen, J. Pahl, A. Causero, G. Ballmann, F. De Proft, S. Harder, *Nat. Catal.* **2018**, *1*, 40–47.
- [21] H. Bauer, M. Alonso, C. Fischer, B. Rösch, H. Elsen, S. Harder, *Angew. Chem. Int. Ed.* **2018**, *57*, 15177–15182; *Angew. Chem.* **2018**, *130*, 15397–15402.
- [22] A. S. S. Wilson, C. Dinoi, M. S. Hill, M. F. Mahon, L. Maron, *Angew. Chem. Int. Ed.* **2018**, *57*, 15500–15504; *Angew. Chem.* **2018**, *130*, 15726–15730.
- [23] H. Bauer, K. Thum, M. Alonso, C. Fischer, S. Harder, *Angew. Chem. Int. Ed.* **2019**, *58*, 4248–4253; *Angew. Chem.* **2019**, *131*, 4292–4297.
- [24] A. S. S. Wilson, M. S. Hill, M. F. Mahon, *Organometallics* **2019**, *38*, 351–360.
- [25] X. Shi, J. Cheng, *Dalton Trans.* **2019**, *48*, 8565–8568.
- [26] J. Martin, C. Knüpfer, J. Eyselien, C. Färber, S. Grams, J. Langer, K. Thum, M. Wiesinger, S. Harder, *Angew. Chem. Int. Ed.* **2020**, *59*, 9102–9112; *Angew. Chem.* **2020**, *132*, 9187–9197.
- [27] X. Shi, C. Hou, L. Zhao, P. Deng, J. Cheng, *Chem. Commun.* **2020**, *56*, 5162–5165.
- [28] P. Stegner, C. Färber, U. Zenneck, C. Knüpfer, J. Eyselien, M. Wiesinger, S. Harder, *Angew. Chem. Int. Ed.* **2021**, *60*, 4252–4258; *Angew. Chem.* **2021**, *133*, 4298–4304.
- [29] J. Martin, J. Eyselien, S. Grams, S. Harder, *ACS Catal.* **2020**, *10*, 7792–7799.
- [30] D. Schuhknecht, T. P. Spaniol, Y. Yang, L. Maron, J. Okuda, *Inorg. Chem.* **2020**, *59*, 9406–9415.
- [31] A. S. S. Wilson, M. S. Hill, M. F. Mahon, C. Dinoi, L. Maron, *Tetrahedron* **2021**, *82*, 131931.
- [32] M. Wiesinger, B. Rösch, C. Knüpfer, J. Mai, J. Langer, S. Harder, *Eur. J. Inorg. Chem.* **2021**, *Accepted Article*, ejic.202100529.
- [33] A. S. S. Wilson, M. S. Hill, M. F. Mahon, C. Dinoi, L. Maron, *Science* **2017**, *358*, 1168–1171.
- [34] P. C. Andrikopoulos, D. R. Armstrong, A. R. Kennedy, R. E. Mulvey, C. T. O'Hara, R. B. Rowlings, *Eur. J. Inorg. Chem.* **2003**, *2003*, 3354–3362.
- [35] D. V. Graham, A. R. Kennedy, R. E. Mulvey, C. T. O'Hara, *Acta Crystallogr. Sect. C* **2006**, *62*, m366–m368.
- [36] D. J. Liptrot, M. S. Hill, M. F. Mahon, *Chem. A Eur. J.* **2014**, *20*, 9871–9874.
- [37] T. X. Gentner, A. R. Kennedy, E. Hevia, R. E. Mulvey, *ChemCatChem* **2021**, *13*, 2371–2378.
- [38] T. X. Gentner, R. E. Mulvey, *Angew. Chem. Int. Ed.* **2021**, *60*, 9247–9262.
- [39] S. D. Robertson, M. Uzelac, R. E. Mulvey, *Chem. Rev.* **2019**, *119*, 8332–8405.
- [40] R. E. Mulvey, F. Mongin, M. Uchiyama, Y. Kondo, *Angew. Chem. Int. Ed.* **2007**, *46*, 3802–3824; *Angew. Chem.* **2007**, *119*, 3876–3899.
- [41] J. M. Gil-Negrete, E. Hevia, *Chem. Sci.* **2021**, *12*, 1982–1992.
- [42] M. Garçon, A. J. P. White, M. R. Crimmin, *Chem. Commun.* **2018**, *54*, 12326–12328.
- [43] M. Garçon, N. W. Mun, A. J. P. White, M. R. Crimmin, *Angew. Chem. Int. Ed.* **2021**, *60*, 6145–6153; *Angew. Chem.* **2021**, *133*, 6210–6218.
- [44] M. Garçon, C. Bakewell, A. J. P. White, M. R. Crimmin, *Chem. Commun.* **2019**, *55*, 1805–1808.
- [45] M. Garçon, C. Bakewell, G. A. Sackman, A. J. P. White, R. I. Cooper, A. J. Edwards, M. R. Crimmin, *Nature* **2019**, *574*, 390–393.
- [46] A. M. Borys, E. Hevia, *Organometallics* **2021**, *40*, 442–447.
- [47] L. C. H. Maddock, A. Kennedy, E. Hevia, *Chim. Int. J. Chem.* **2020**, *74*, 866–870.
- [48] M. Garçon, N. W. Mun, A. J. P. White, M. R. Crimmin, *Angew. Chemie Int. Ed.* **2021**, *60*, 6145–6153.
- [49] F. Rekhroukh, W. Chen, R. K. Brown, A. J. P. White, M. R. Crimmin, *Chem. Sci.* **2020**, *11*, 7842–7849.
- [50] S. Lau, A. J. P. White, I. J. Casely, M. R. Crimmin, *Organometallics* **2018**, *37*, 4521–4526.
- [51] P. Büschelberger, D. Gärtner, E. Reyes-Rodriguez, F. Kreyenschmidt, K. Koszinowski, A. Jacobi von Wangelin, R. Wolf, *Chem. A Eur. J.* **2017**, *23*, 3139–3151.
- [52] L. Garcia, M. F. Mahon, M. S. Hill, *Organometallics* **2019**, *38*, 3778–3785.
- [53] H. Elsen, C. Färber, G. Ballmann, S. Harder, *Angew. Chem.* **2018**, *130*, 7274–7278; *Angew. Chem. Int. Ed.* **2018**, *57*, 7156–7160.
- [54] H. Elsen, J. Langer, G. Ballmann, M. Wiesinger, S. Harder, *Chem. A Eur. J.* **2021**, *27*, 401–411.
- [55] H. Elsen, J. Langer, M. Wiesinger, S. Harder, *Organometallics* **2020**, *39*, 4238–4246.
- [56] D. R. Armstrong, W. Clegg, R. P. Davies, S. T. Liddle, D. J. Linton, P. R. Raithby, R. Snaith, A. E. H. Wheatley, *Angew. Chem. Int. Ed.* **1999**, *38*, 3367–3370; *Angew. Chem.* **1999**, *111*, 3568–3570.
- [57] J. Haywood, A. E. H. Wheatley, *Dalton Trans.* **2008**, 3378–3397.
- [58] D. Martin, K. Beckerle, S. Schnitzler, T. P. Spaniol, L. Maron, J. Okuda, *Angew. Chem. Int. Ed.* **2015**, *54*, 4115–4118; *Angew. Chem.* **2015**, *127*, 4188–4191.
- [59] A. V. Timofeenko, *J. Math. Sci.* **2009**, *162*, 710–729.
- [60] S. Harder, J. Spielmann, J. Intemann, H. Bandmann, *Angew. Chem. Int. Ed.* **2011**, *50*, 4156–4160; *Angew. Chem.* **2011**, *123*, 4242–4246.
- [61] S. Hayashi, *J. Alloys Compd.* **1997**, *248*, 66–69.
- [62] P. C. M. M. Magusin, W. P. Kalisvaart, P. H. L. Notten, R. A. van Santen, *Chem. Phys. Lett.* **2008**, *456*, 55–58.
- [63] M. Kaupp, O. L. Malkina, V. G. Malkin, P. Pyykkö, *Chem. A Eur. J.* **1998**, *4*, 118–126.
- [64] M. Kaupp, O. L. Malkina, *J. Chem. Phys.* **1998**, *108*, 3648–3659.

- [65] M. Wiesinger, B. Maitland, H. Elsen, J. Pahl, S. Harder, *Eur. J. Inorg. Chem.* **2019**, 2019, 4433–4439.
- [66] J. Intemann, J. Spielmann, P. Sirsch, S. Harder, *Chem. A Eur. J.* **2013**, *19*, 8478–8489.
- [67] X. Y. Zhang, H. Z. Du, D. D. Zhai, B. T. Guan, B. T. Guan, *Org. Chem. Front.* **2020**, *7*, 1991–1996.
- [68] J.-M. Begouin, M. Niggemann, *Chem. A Eur. J.* **2013**, *19*, 8030–8041.
- [69] J. Penafiel, L. Maron, S. Harder, *Angew. Chem. Int. Ed.* **2015**, *54*, 201–206; *Angew. Chem.* **2015**, *127*, 203–208.
- [70] K. Thum, A. Friedrich, J. Pahl, H. Elsen, J. Langer, S. Harder, *Chem. A Eur. J.* **2021**, *27*, 2513–2522.
- [71] J. Pahl, S. Brand, H. Elsen, S. Harder, *Chem. Commun.* **2018**, *54*, 8685–8688.
- [72] J. Pahl, T. E. Stennett, M. Volland, D. M. Guldi, S. Harder, *Chem. A Eur. J.* **2019**, *25*, 2025–2034.
- [73] J. Pahl, A. Friedrich, H. Elsen, S. Harder, *Organometallics* **2018**, *37*, 2901–2909.
- [74] L. Garcia, M. D. Anker, M. F. Mahon, L. Maron, M. S. Hill, *Dalton Trans.* **2018**, *47*, 12684–12693.
- [75] A. Friedrich, J. Pahl, H. Elsen, S. Harder, *Dalton Trans.* **2019**, *48*, 5560–5568.
- [76] M. Schorpp, I. Krossing, *Chem. Sci.* **2020**, *11*, 2068–2076.
- [77] S. Tussing, K. Kaupmees, J. Paradies, *Chem. A Eur. J.* **2016**, *22*, 7422–7426.
- [78] R. Wang, M. Ma, X. Gong, G. B. Panetti, X. Fan, P. J. Walsh, *Org. Lett.* **2018**, *20*, 2433–2436.
- [79] D. Nanni, P. Pareschi, J. C. Walton, *J. Chem. Soc. Perkin Trans. 2* **2002**, 1098–1104.
- [80] J. R. Miecznikowski, R. H. Crabtree, *Polyhedron* **2004**, *23*, 2857–2872.
- [81] M. Westerhausen, *Inorg. Chem.* **1991**, *30*, 96–101.

Manuscript received: July 15, 2021
Revised manuscript received: August 9, 2021
Accepted manuscript online: August 19, 2021
Version of record online: ■■■, ■■■■

FULL PAPERS



*M. Wiesinger, C. Knüpfer, Dr. H. Elsen, J. Mai, Dr. J. Langer, Prof. S. Harder**

1 – 12

Heterometallic Mg–Ba Hydride Clusters in Hydrogenation Catalysis



Heterometallic catalysis: Three different Mg/Ba hydride clusters have been prepared and were studied in the solid state and in solution. Coop-

erative effects between Mg and Ba in hydrogenation catalysis have been evaluated.
